METHOD

Development of a modified RNA circularization system to improve circRNA-based protein expression in mammalian cells

MINGTING CUI,[1] SHUNRAN LI,[1] YUHANG HAN,[2] MINCHAO LI,[1] ZIRONG HAN,[1,3,4] JUN QIAN,[1,3,4] ZHI XIE,[5] and CAIJUN SUN[1,3,4]

[1]School of Public Health (Shenzhen), Sun Yat-sen University, Shenzhen 518107, China
[2]School of Pharmaceutical Sciences (Shenzhen), Sun Yat-sen University, Shenzhen 518107, China
[3]Key Laboratory of Tropical Disease Control (Sun Yat-sen University), Ministry of Education, Guangzhou 514400, China
[4]Shenzhen Key Laboratory of Pathogenic Microbes and Biosafety, Shenzhen Campus of Sun Yat-sen University, Shenzhen 518107, China
[5]State Key Laboratory of Ophthalmology, Zhongshan Ophthalmic Center, Sun Yat-sen University, Guangzhou 510060, China

ABSTRACT

Circular RNA (circRNA) is emerging as a highly promising technology in various biomedical applications, offering advantages over traditional linear RNA. The Twister-optimized RNA for the durable overexpression (Tornado) system has been widely investigated for generating circRNAs in mammalian cells; however, the use of the Tornado system for large RNA inserts, especially those containing the internal ribosome entry site (IRES) sequences, is hindered by low circularization efficiency and limited circRNA abundance. Therefore, developing novel strategies to enhance RNA circularization in cells is of critical importance. In this study, we present a modified Tornado system that significantly improves circRNA-based protein expression by incorporating an optimal distance between the IRES and the upstream CMV promoter. Furthermore, we elucidate the dual roles of HRV-B3 IRES in mammalian cells, demonstrating its negative regulatory effect on RNA abundance and its positive contribution to RNA circularization. Additionally, the integration of a truncated 5′ long terminal repeat (LTR) from HIV-1 upstream of the HRV-B3 IRES, combined with the woodchuck hepatitis virus post-transcriptional regulatory element (WPRE), further enhances transcriptional efficiency in the Tornado system. This modified system holds great potential for advancing circRNA-based therapeutics and vaccines, and these findings provide valuable insights for refining the Tornado system and designing regulatory elements in synthetic biology applications.

Keywords: circRNA; Tornado system; IRES; therapeutics; synthetic biology

INTRODUCTION

mRNA-based therapeutics and vaccines have emerged as a promising technology across diverse biomedical applications. However, the therapeutic potential is significantly constrained by the short half-life of linear mRNAs due to its inherent instability in cytoplasm. This limitation can be effectively addressed through the use of circular RNAs (circRNAs) (Wesselhoeft et al. 2018), which are resistant to exonucleolytic degradation (Ibrahim et al. 2008). The remarkable stability of circRNAs makes them an attractive alternative for achieving sustained protein expression, and thus it is of great potential for advancing circRNA-based therapeutics and vaccines (Qu et al. 2022; Yue et al. 2024). Unlike linear mRNAs that require a 5′ cap structure for translation initiation, circRNAs use an internal ribosome entry site (IRES) to recruit the translational machinery (Chen and Sarnow 1995). Current methodologies for circRNA synthesis primarily involve two approaches: enzymatic ligation of 3′ and 5′ ends, and utilization of permuted self-splicing introns (Puttaraju and Been 1992; Obi and Chen 2021; Qu et al. 2022). In particular, modified group I introns using a permuted intron–exon (PIE) arrangement have demonstrated significant potential. In this strategy, target RNAs are flanked by two exons, with the 3′ half of the intron positioned at the 5′ end and the 5′ half at the 3′ end. Splicing subsequently circularizes the RNA through exon ligation (Puttaraju and Been 1992).

Corresponding authors: suncaijun@mail.sysu.edu.cn, xiezhi@gmail.com
Handling editor: Ling-Ling Chen
Article is online at http://www.rnajournal.org/cgi/doi/10.1261/rna.080733.125.

Currently, circRNA synthesis methods include cell-free system and in-cell system. While significant progress has been made in cell-free circRNA synthesis system, critical limitations hinder its widely clinical applications. (1) Immunogenic byproducts (such as linear RNA contaminants) trigger robust cellular immune responses (Wesselhoeft et al. 2019). (2) The residual unmodified circRNAs (non-m^{6}A modification) can activate RIG-I via K63-polyubiquitin–mediated signaling, thus inducing MAVS filamentation, IRF3 dimerization, and interferon production (Chen et al. 2019). (3) Lack of endogenous RNA-binding proteins: Cell-free synthesized circRNAs lack host-derived RNA-binding proteins that tag circRNAs as "self" to reduce immunogenicity (Chen et al. 2017). Notably, in-cell circRNA synthesis—using human-derived introns to template foreign sequences—mitigates this immunogenicity. Thus, while cell-free systems achieve higher circRNA yields (Wesselhoeft et al. 2018), in-cell circRNA synthesis is promising for minimizing excessive immune activation in therapeutic and vaccine applications. However, in-cell circRNA synthesis still faces challenges in terms of abundance and circularization efficiency. Naturally occurring circRNAs in eukaryotic cells are typically generated through a mechanism involving complementary Alu elements, where base-pairing between these sequences facilitates splice site approximation through a protein-bridging mechanism (Dubin et al. 1995; Jeck et al. 2013; Liang and Wilusz 2014; Zhang et al. 2014; Ivanov et al. 2015; Li et al. 2015). Several innovative approaches have been developed to enhance circRNA production. For example, a reporter plasmid incorporating exons 14–17 of the *SMARCA5* gene was engineered with green fluorescent protein (GFP) and IRES sequences inserted into exons 15 and 16, respectively, successfully generating circRNA through the alternative splicing factor Quaking (QKI) (Conn et al. 2015). The *ZKSCAN* intron system has also been used for circularizing GFP and IRES sequences, enabling efficient screening of functional circRNA IRES elements (Kramer et al. 2015; Chen et al. 2021). Commercial circularization vectors, such as the pLC5-ciR vector containing optimized Alu elements and QKI binding sites, have demonstrated improved efficiency, achieving over 50-fold upregulation of circCDK13 levels relative to endogenous expression (Huang et al. 2024).

In contrast to conventional in-cell RNA circularization methods, an alternative approach harnessing transfer RNA (tRNA) splicing machinery exhibit superior efficiency. The tRNA splicing mechanism was first described in 1983, with precursor tRNAs identified to harbor distinctive termini: a 5′-hydroxyl group and a 2′,3′-cyclic phosphate at the 3′ end (Filipowicz and Shatkin 1983; Laski et al. 1983). This foundational work culminated in the discovery of RtcB as the essential ligase mediating junction of these modified termini (Tanaka et al. 2011). Based on these findings, researchers developed an in-cell platform to engineer circRNAs—including functional RNA aptamers—in human cells (Lu et al. 2015). However, practical utility of this system was constrained by its low yield. A breakthrough emerged with the Twister-optimized RNA for durable overexpression (Tornado) system (Litke and Jaffrey 2019), which integrates two flanking Twister ribozymes. These ribozymes enable rapid autocatalytic cleavage, bypassing slow enzymatic ligation steps and dramatically improving circRNA output. Unlike the above-mentioned intron-driven circularization systems, which can produce scarless circRNAs that maintain native sequence integrity and thereby eliminate vector-derived artifacts (Chen et al. 2025), the Tornado system usually leaves a sequence scar on the resulting circRNAs, which may affect their structure, stability, or biological function. Initially designed for RNA aptamer circularization, the Tornado platform has since been expanded to protein-coding applications. Tornado-based circRNA expression is quite high for small RNAs like aptamers but significantly reduced for larger RNAs, such as coding sequences. Most notably, its recent adaptation to circularize large RNA constructs containing IRES and open reading frames (ORFs) has established the Tornado translation system as a robust tool for protein synthesis, outperforming the *ZKSCAN1* backsplicing method in comparative studies (Unti and Jaffrey 2024). Despite these advancements, current RNA circularization methods still suffer from relatively low circRNA abundance, and produce transcripts at significantly lower levels compared to linear mRNA systems, highlighting the need for continued innovation in RNA circularization technologies.

In this study, we systematically investigated a novel strategy to enhance protein expression from Tornado translation system–generated circRNA and elucidated the regulatory mechanism of IRES elements in mammalian cells. Our findings demonstrated that the HRV-B3 IRES sequence exerts a *cis*-acting inhibitory effect on RNA abundance, independent of transcription termination. We also found for the first time that appropriate insertion of a spacer sequence between the HRV-B3 IRES and upstream promoter significantly enhanced the downstream gene expression. Our findings provide valuable guidance to modify the Tornado translation system for improving circRNA-based protein expression, and also offer fundamental insights for the rational design of regulatory elements in synthetic biology applications.

RESULTS

Tornado system incorporating the optimized HRV-B3 IRES yielded high level of protein expression

circRNAs synthesized typically use a group I intron-derived backbone with PIE arrangements, as exemplified by the engineered Anabaena PIE system. This system comprises a 3′ intron, exon 2, exon 1, and a 5′ intron in sequential

order. A key feature of this design is the inclusion of spacer–spacer complementary sequences that facilitate the formation of a protected "splicing bubble"—a structural motif in which catalytic intronic sequences are flanked by homologous regions (Fig. 1A, upper panel; Wesselhoeft et al. 2018). In addition, to enable cap-independent translation, an IRES element is engineered upstream of an ORF sequence. Recent advancements use an optimized IRES derived from human rhinovirus B3 (HRV-B3), which incorporates an eIF4G-binding aptamer critical for ribosome recruitment, along with a 5′ UTR PABPv2 spacer and a full HBA1 3′ UTR to maximize translational output (Chen et al. 2023). These flanking elements not only enhance circRNA circularization efficiency but also stabilize RNA secondary structures required for sustained protein synthesis.

To identify elements that can potentially improve protein expression, we synthesized circRNAs encoding enhanced GFP using different translation frameworks. These circRNAs were generated through in vitro transcription (IVT) and intron-assisted splicing. One construct with a full length of 1629 nt, featured an HRV-B3 IRES with its spacer elements, while the other measured 1655 nt in length and used Coxsackievirus B3 (CVB3) IRES with spacers (Fig. 1A). Following transfection into HEK293T cells, GFP expression was quantified by flow cytometry, and results showed that cells transfected with the construct containing HRV-B3 IRES exhibited significantly lower GFP levels compared to those transfected with the construct containing CVB3 IRES (Fig. 1B).

The Tornado system comprises the following core components: a 5′ P3 Twister U2A ribozyme, complementary sequences (5′ and 3′), and a 3′ P1 Twister ribozyme. Following transcription, the ribozymes undergo autocatalytic self-cleavage, enabling the 5′ and 3′ RNA termini to be spatially aligned via hybridization of the complementary sequences, and subsequently ligated by the RNA ligase RtcB. Next, to evaluate the performance of HRV-B3 IRES in the Tornado system, we constructed two plasmids: pcDNA3-Tornado-HRV-B3_IRES-GFP and pcDNA3-Tornado-CVB3_IRES-GFP (Fig. 1C). The IRES sequences were adjacent to the upstream sequence of the GFP gene to maximize translation efficiency. Surprisingly, the Tornado system incorporating HRV-B3 IRES with its spacer elements yielded higher levels of GFP expression than that with CVB3 IRES (Fig. 1D).

To investigate whether this enhanced protein expression was because of increased RNA levels, we compared the relative GFP RNA levels in cells transfected with pcDNA3-Tornado-HRV-B3_IRES-GFP and pcDNA3-Tornado-CVB3_IRES-GFP. Remarkably, cells transfected with the HRV-B3 IRES construct exhibited >40-fold higher GFP RNA levels (including both linear and circular GFP RNAs) than those transfected with the CVB3 IRES construct (Fig. 1E). This demonstrates that the HRV-B3 IRES-based Tornado system, which integrates spacer elements (PABPv2 and HBA1 UTRs), correlates with substantially higher RNA abundance, thereby driving enhanced protein translation. This characteristic aligns with our goal of optimizing circRNA-based protein expression. Consequently, the Tornado system using the same HRV-B3 IRES element was selected for subsequent experiments.

Then, we integrated HRV-B3 IRES with its spacer elements and a reporter gene (e.g., GFP or luciferase) into the Tornado translation system (Fig. 1F). After transfecting HEK293T cells, we used convergent and divergent primers to detect linear mRNA transcripts and circRNAs. Only cDNA derived from circRNAs produced a distinct band when amplified with divergent primers in agarose gel electrophoresis, confirming successful RNA circularization by the Tornado system (Fig. 1G). Consistent with previous findings, the Tornado translation system yielded lower protein levels than the linear mRNA system (Fig. 1H,I), though it should be noted that the GFP signal observed in the Tornado system may partially derive from linear RNA products. Similarly, luciferase (Luci) assay also revealed minimal Luci expression in the Tornado system, with pcDNA3-Tornado-IRES-Luci producing ∼1/100 Luci activity of the pcDNA3-Luci construct (Fig. 1J). This discrepancy was likely attributable to the inherently lower activity of IRES-mediated translation compared to cap-dependent mechanisms. These results suggested that the Tornado system can circularize RNAs but correlates with lower RNA levels than linear mRNA system, and thus it is of great importance to optimize Tornado system for improving circRNA-based protein expression.

pCDH vector-based Tornado system enhances circRNA-based protein expression

During the construction of lentiviruses containing the GFP gene within the Tornado system using the pCDH shuttle plasmid (pCDH-CMV-MCS-EF1-Puro, hereafter referred to as pCDH), we observed unexpectedly high protein production (Fig. 2A,B). In the pCDH-based lentiviral vector system, the Rous sarcoma virus (RSV) promoter upstream of the truncated 5′ long terminal repeat (LTR) functions as a promoter to initiate transcription, and the transcription process terminates at the 3′ end of the 3′ LTR. Unless otherwise specified, the subsequent 5′ LTR refers to the RSV promoter and the truncated 5′ LTR. To further investigate this observation, we transiently transfected HEK293T cells with either pcDNA3 or pCDH plasmids carrying the Tornado system or a linear mRNA system. As expected, the linear mRNA system in the pcDNA3 vector, which includes a CMV enhancer, exhibited higher protein expression than the pCDH vector (Fig. 2C,D). However, for the Tornado system, the pCDH vector produced significantly more GFP expression than that of pcDNA3 vector (Fig. 2C,D). Since the identical Tornado system (including the

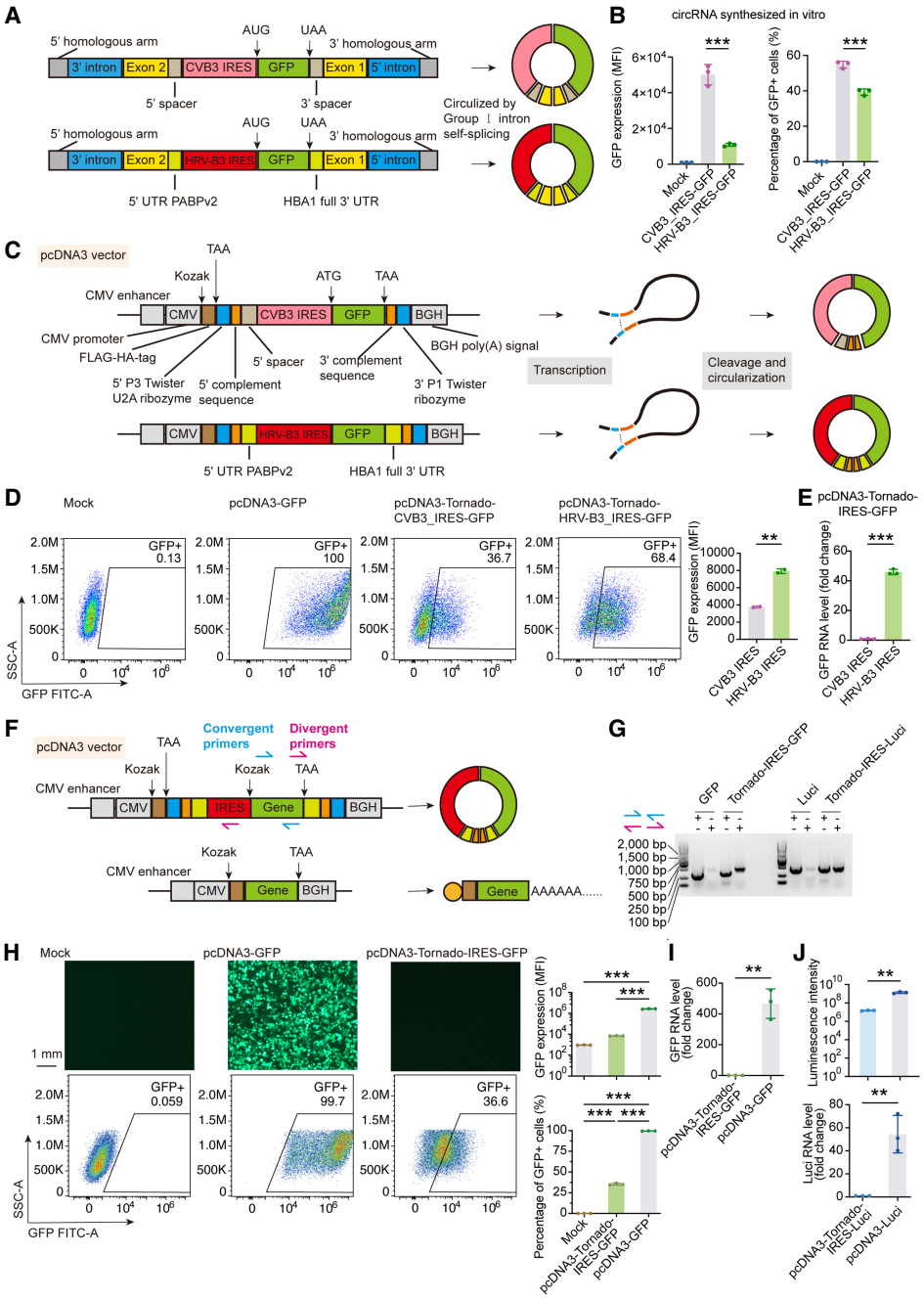

FIGURE 1. Tornado system incorporating the optimized HRV-B3 IRES yielded high level of protein expression. (*A*) Design of circRNA circularization via group I intron autocatalysis in vitro. (*B*) Flow cytometry analysis was performed to measure mean fluorescence intensity (MFI) of GFP expression and percentage of GFP-positive cells in HEK293T cells transfected with the construct containing CVB3 IRES or the construct containing HRV-B3 IRES for 48 h. Untreated cells served as a negative control. (*C*) Design of Tornado translation system in pcDNA3 vector. (*D*) Flow cytometry analysis of GFP expression in HEK293T cells transfected with pcDNA3-GFP, pcDNA3-Tornado-CVB3_IRES-GFP, or pcDNA3-Tornado-HRV-B3_IRES-GFP for 48 h. Untreated cells served as a negative control. (*E*) Relative GFP RNA levels measured by RT-qPCR in HEK293T cells transfected with pcDNA3-Tornado-CVB3_IRES-GFP or pcDNA3-Tornado-HRV-B3_IRES-GFP. (*F*) Design of Tornado translation system featuring a 5′ UTR PABPv2 spacer, HRV-B3 IRES (with an eIF4G-binding aptamer), and a full HBA1 3′ UTR. The arrows indicate the primer design for PCR analysis. (*G*) Agarose gel electrophoresis of PCR products amplified from cDNA, which was reverse-transcribed from RNA harvested from HEK293T cells transfected with pcDNA3-GFP, pcDNA3-Tornado-IRES-GFP, pcDNA3-Luci, or pcDNA3-Tornado-IRES-Luci. Both convergent and divergent primers were used. (*H*) Transfection efficiency and GFP expression levels in HEK293T cells transfected with 1 µg of pcDNA3-GFP or pcDNA3-Tornado-IRES-GFP for 48 h. (*I*) Relative GFP RNA levels in HEK293T cells transfected with pcDNA3-Tornado-IRES-GFP or pcDNA3-GFP. (*J*) Luminescence and relative Luci RNA levels in HEK293T cells transfected with pcDNA3-Tornado-IRES-Luci or pcDNA3-Luci. (Luci) Luciferase. The data are shown as mean ± SD of at least three independent experiments, and *P*-values of <0.05 were deemed statistically significant. (**) $P < 0.01$; (***) $P < 0.001$.

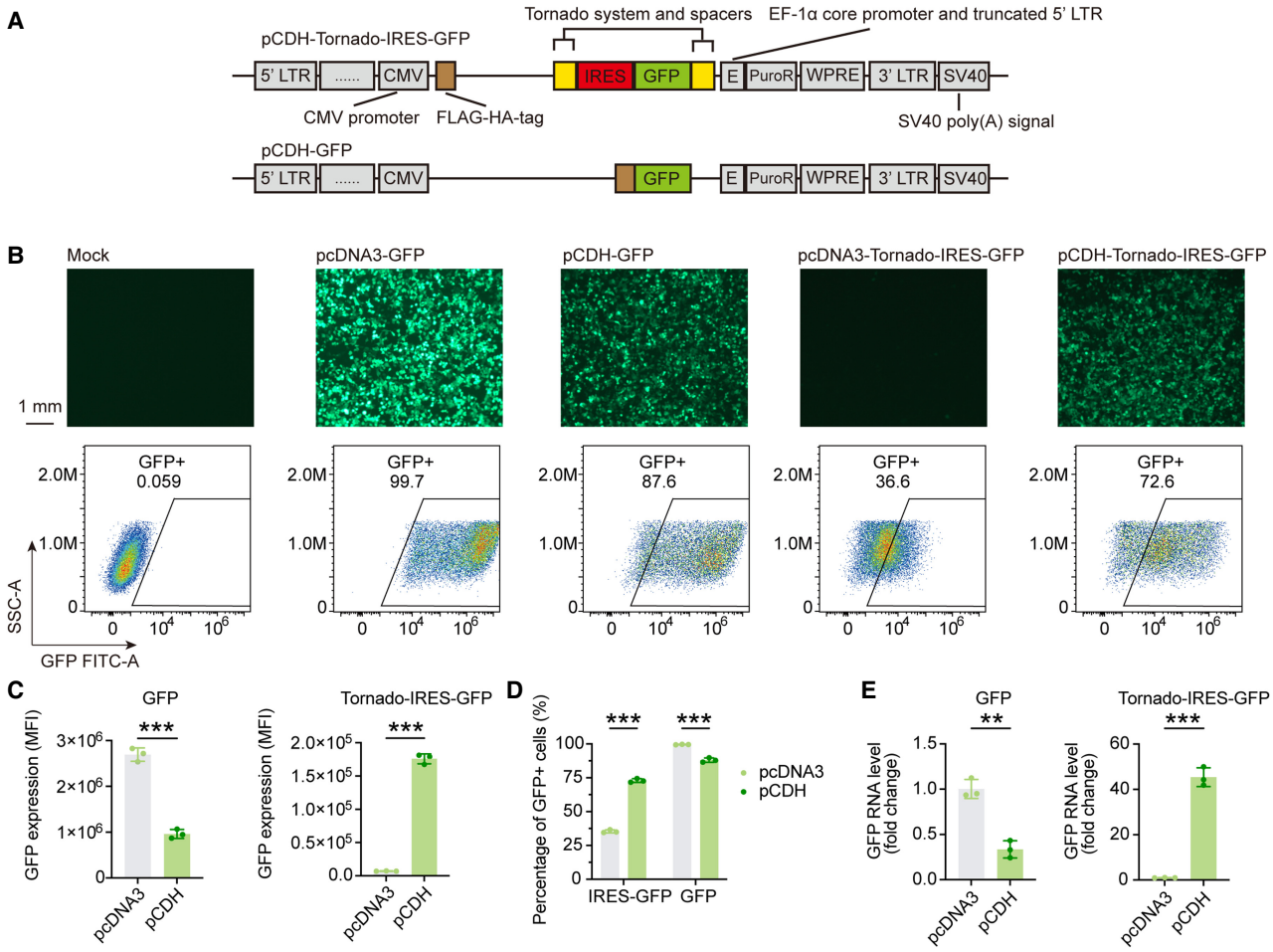

FIGURE 2. pCDH vector-based Tornado system enhances circRNA-based protein expression. (*A*) Design of the Tornado translation system based on pCDH vector. The symbol (……) represents key elements, including the HIV-1 packaging signal (HIV-1 Ψ), Rev response element (RRE) for Rev-dependent nuclear export, an antigenic peptide (amino acids 655–669 of HIV gp41), and the central polypurine tract/termination sequence of HIV-1 (cPPT/CTS). (*B–D*) GFP expression levels (MFI) and percentage of GFP-positive cells in HEK293T cells transfected with pcDNA3-GFP, pCDH-GFP, pcDNA3-Tornado-IRES-GFP, or pCDH-Tornado-IRES-GFP. (*E*) Relative GFP RNA levels in HEK293T cells transfected with indicated vectors for 48 h. The data are shown as mean ± SD of at least three independent experiments, and *P*-values of <0.05 were deemed statistically significant. (**) $P < 0.01$; (***) $P < 0.001$.

same HRV-B3 IRES element) was used in these constructs, the observed protein expression enhancement likely reflects differences in the pCDH vector system itself.

To further test this hypothesis, we measured relative GFP RNA levels using reverse transcription quantitative PCR (RT-qPCR). For the linear mRNA system, the pCDH vector showed lower GFP RNA levels than the pcDNA3 vector, whereas the opposite was observed for the Tornado system (Fig. 2E). These findings indicated that the pCDH vector increased RNA abundance in the context of the Tornado system.

The transition from the pcDNA3 to the pCDH vector differentially impacts RNA abundance depending on the translation system. This effect appears to be influenced by the presence of the Tornado system and IRES. Previous studies have shown that IRES can significantly reduce RNA polymerase II activity in adjacent regions (Slobodin et al. 2020). Our data suggest that specific elements within the pCDH vector may counteract this effect, upregulate RNA abundance by modulating the activity of the Tornado system or the IRES. This discovery highlighted the potential of the pCDH vector for optimizing circRNA-based protein expression system.

Dual roles of HRV-B3 IRES in negative RNA-abundance regulation and positive RNA circularization

To investigate whether IRES contributes to RNA reduction, we replaced the HRV-B3 IRES sequence (666 bp, including the eIF4G-binding aptamer) with an mCherry sequence (708 bp) in the plasmid constructs (Fig. 3A). The resulting constructs exhibited comparable lengths, with a negligible size difference of 42 bp (<0.68% of the total plasmid

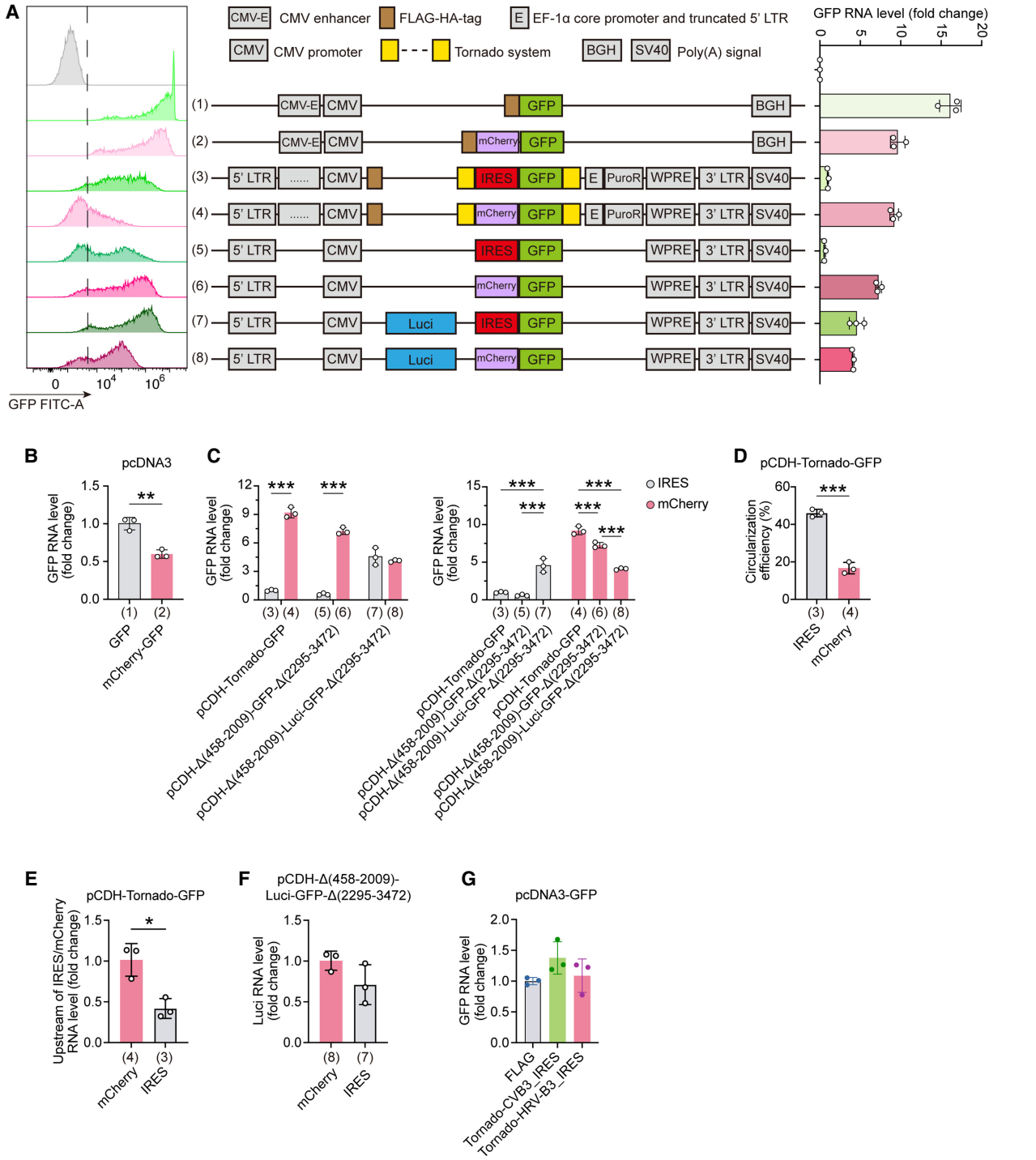

FIGURE 3. Dual roles of HRV-B3 IRES in negative RNA-abundance regulation and positive RNA circularization. (*A*, *left*) Flow cytometry histogram plots. (*Middle*) Schematic of plasmids containing either IRES or mCherry. All the plasmids are numbered. The symbol (……) represents key elements, including HIV-1 Ψ, RRE, gp41 peptide, and cPPT/CTS. (*Right*) Relative GFP RNA levels in HEK293T cells transfected with the plasmids shown in the *middle* panel. (*B*) Relative GFP RNA levels in HEK293T cells transfected with pcDNA3-GFP or pcDNA3-mCherry-GFP. (*C*) Comparison of relative GFP RNA levels in HEK293T cells transfected with plasmids containing HRV-B3 IRES or mCherry. (*D*) Circularization efficiency of RNA transcribed from pCDH-Tornado-GFP with IRES or mCherry inserted upstream of GFP. (*E*) The RNA levels upstream of IRES or mCherry in HEK293T cells transfected with pCDH-Tornado-IRES-GFP or pCDH-Tornado-mCherry-GFP for 48 h. (*F*) Relative Luci RNA levels in HEK293T cells transfected with pCDH-Δ(458-2009)-Luci-IRES-GFP-Δ(2295-3472) or pCDH-Δ(458-2009)-Luci-mCherry-GFP-Δ(2295-3472) for 48 h. (*G*) Relative GFP RNA levels in HEK293T cells cotransfected with pcDNA3-GFP and either pcDNA3-FLAG (negative control), pcDNA3-Tornado-CVB3_IRES, or pcDNA3-Tornado-HRV-B3_IRES for 48 h. The data are shown as mean ± SD of at least three independent experiments, and *P*-values of <0.05 were deemed statistically significant. (*) $P<0.05$; (**) $P<0.01$; (***) $P<0.001$.

length). This minimal size variation ensured equivalent molar plasmid amounts when equal masses were transfected, thereby normalizing comparisons between HRV-B3 IRES-positive and HRV-B3 IRES-negative constructs. To exclude promoter-like activity in these sequences, both the HRV-B3 IRES and mCherry regions were analyzed using Promoter 2.0 (https://services.healthtech.dtu.dk/services/Promoter-2.0/) (Knudsen 1999), which confirmed the absence of predicted promoter motifs (output: "No promoter predicted"). Moreover, to exclude that mCherry itself does not activate transcription, we cloned the mCherry gene into the pcDNA3-GFP plasmid, positioning it upstream of the GFP gene. After transfecting HEK293T cells, we measured relative GFP RNA levels using RT-qPCR, and results showed that the GFP RNA levels in pcDNA3-mCherry-GFP (Plasmid 2) were lower than those in pcDNA3-GFP (Plasmid 1) (Fig. 3B). This reduction in RNA levels may be due to the increased length of the transcription template or the lower molarity for transfection.

Next, we replaced the HRV-B3 IRES sequence in pCDH-Tornado-IRES-GFP (Plasmid 3) with the mCherry sequence, creating pCDH-Tornado-mCherry-GFP (Plasmid 4). Transfection of HEK293T cells revealed that the relative GFP RNA levels in pCDH-Tornado-mCherry-GFP (Plasmid 4) were significantly higher than those in pCDH-Tornado-IRES-GFP (Plasmid 3) (Fig. 3C), suggesting that the HRV-B3 IRES played a role in decreased RNA abundance.

To further investigate the RNA-reducing effects mediated by IRES and mCherry elements, we removed nonessential sequences from the pCDH vector (Fig. 3A). The deleted regions included the following: (1) the sequence between the truncated 5′ LTR from HIV-1 and the CMV promoter (nucleotides 458–2009 in pCDH vector; the first nucleotide of the HIV-1 Ψ sequence is designated as nucleotide 458); (2) the Tornado system; and (3) a region encompassing the core promoter for human elongation factor EF-1α (EF-1α core promoter), the truncated 5′ LTR from human T-cell leukemia virus (HTLV) type 1, and the puromycin N-acetyltransferase (PuroR) gene (nucleotides 2295–3472 in pCDH vector). The resulting plasmids were named pCDH-Δ(458-2009)-IRES-GFP-Δ(2295-3472) (Plasmid 5) and pCDH-Δ(458-2009)-mCherry-GFP-Δ(2295-3472) (Plasmid 6). After transfecting HEK293T cells, we measured relative GFP RNA levels using RT-qPCR. Both constructs exhibited reduced GFP RNA levels compared to the original pCDH vectors (transfected at equal mass but higher molarity), but the mCherry-containing plasmid consistently showed higher GFP RNA levels than the HRV-B3 IRES-containing plasmid (Fig. 3C). This indicated that the deleted regions potentially enhance transcription or RNA stability in the presence of HRV-B3 IRES. Additionally, circularization efficiency was significantly higher in pCDH-Tornado-IRES-GFP (Plasmid 3) (>40%) compared to pCDH-Tornado-mCherry-GFP (Plasmid 4) (<20%) (Fig. 3D), further highlighting the dual roles of HRV-B3 IRES in negative RNA-abundance regulation and positive RNA circularization.

Then, to investigate whether HRV-B3 IRES negatively regulates RNA synthesis via transcription termination, we designed a pair of primers specific to the sequence between the CMV promoter and the 5′ Tornado system. If HRV-B3 IRES promotes transcription termination, the transcripts upstream of the IRES would be more abundant than those downstream. However, in HEK293T cells transfected with pCDH-Tornado-IRES-GFP (Plasmid 3), the RNA level upstream of the IRES was lower than in cells transfected with pCDH-Tornado-mCherry-GFP (Plasmid 4), corresponding to the reduced relative GFP RNA levels (Fig. 3C–E). Additionally, no significant difference in relative Luci RNA levels was observed between pCDH-Δ(458-2009)-Luci-IRES-GFP-Δ(2295-3472) (Plasmid 7) and pCDH-Δ(458-2009)-Luci-mCherry-GFP-Δ(2295-3472) (Plasmid 8) (Fig. 3F). These results, consistent with the relative GFP RNA levels in transfected HEK293T cells, demonstrate that HRV-B3 IRES does not decrease RNA synthesis through transcription termination. We also investigated whether the HRV-B3 IRES from different derivations affects the level of RNA abundance. HEK293T cells were cotransfected with pcDNA3-GFP (Plasmid 1) and either HRV-B3 IRES, CVB3 IRES in the Tornado system, or pcDNA3-FLAG as a mock control. No significant differences in relative GFP RNA levels were observed among these groups, indicating that IRES does not negatively regulate RNA abundance when plasmids were used as template through *trans*-acting mechanisms (Fig. 3G).

Furthermore, we inserted a luciferase (Luci) sequence (1653 bp) upstream of the IRES in pCDH-Δ(458-2009)-IRES-GFP-Δ(2295-3472) (Plasmid 5) [designated as pCDH-Δ(458-2009)-Luci-IRES-GFP-Δ(2295-3472) (Plasmid 7)] and upstream of mCherry in pCDH-Δ(458-2009)-mCherry-GFP-Δ(2295-3472) (Plasmid 6) [designated as pCDH-Δ(458-2009)-Luci-mCherry-GFP-Δ(2295-3472) (Plasmid 8)] (Fig. 3A). For the mCherry construct, the addition of the Luci sequence reduced relative GFP RNA levels, likely due to the increased length of the transcription template or the lower molarity for transfection (Fig. 3C). In contrast, for the HRV-B3 IRES construct, the Luci sequence significantly increased relative GFP RNA levels. Remarkably, the GFP RNA levels in pCDH-Δ(458-2009)-Luci-IRES-GFP-Δ(2295-3472) (Plasmid 7) were comparable to those in pCDH-Δ(458-2009)-Luci-mCherry-GFP-Δ(2295-3472) (Plasmid 8) (Fig. 3C). Notably, IRES-containing mRNAs with the upstream insertions exhibited faster degradation rates compared to their IRES-negative counterparts with identical upstream sequences (Slobodin et al. 2020). These findings demonstrate that strategic insertion of additional sequences (e.g., luciferase) between the CMV promoter and IRES element can effectively mitigate the RNA-reduction effect of IRES element.

Increased distance between IRES and upstream promoter mitigates RNA-abundance downregulation

To systematically test this hypothesis, we generated a series of plasmids containing various sequence intervals between the CMV promoter and HRV-B3 IRES element, with or without the Luci sequence (Fig. 4A). To be noted, when the equal masses of plasmids were transfected, the molecular amounts of DNA with additional inserted sequences were fewer relative to those without additional insertion constructs (calculated based on plasmid molecular weights). However, after transfecting these plasmids into HEK293T cells, we found that the inclusion of the Luci sequence upstream of the IRES significantly increased GFP expression (Fig. 4B,C).

When the Tornado system elements were removed [comparing pCDH-Δ(458-2009)-IRES-GFP-Δ(2295-3472) (Plasmid 5) to pCDH-Δ(458-2009)-Tornado-IRES-GFP-Δ(2295-3472) (Plasmid 10)], we observed that the shorter distance between the HRV-B3 IRES and the CMV promoter correlated with higher GFP RNA levels (Fig. 4D). This implies that the Tornado system reduces GFP RNA levels, potentially due to increased degradation of RNA lacking a 5′ cap and a 3′ poly(A) tail. Notably, the GFP RNA levels in pCDH-Δ(458-2009)-Luci-IRES-GFP-Δ(2295-3472) (Plasmid 7) were higher than those in pcDNA3-Luci-Tornado-IRES-GFP (Plasmid 11), suggesting that the 5′ LTR promoter and woodchuck hepatitis virus post-transcriptional regulatory element (WPRE) may enhance transcription activity or transcript stability in conjunction with the HRV-B3 IRES (Fig. 4E). Additionally, reducing the distance between the 5′ LTR and the IRES [comparing pCDH-Δ(458-2009)-Tornado-IRES-GFP-Δ(2295-3472) (Plasmid 10) to pCDH-Tornado-IRES-GFP (Plasmid 3)] resulted in lower GFP RNA levels (Fig. 4D). Furthermore, constructs with both the 5′ LTR and CMV promoters positioned far from the IRES exhibited higher GFP RNA levels than those with only the 5′ LTR promoter distant from the IRES, as evidenced by the comparative analysis between pCDH-Δ(458-2009)-Luci-Tornado-IRES-GFP-Δ(2295-3472) (Plasmid 12) and pCDH-Tornado-IRES-GFP (Plasmid 3) (Fig. 4F). However, inserting a long sequence between the 5′ LTR and CMV promoter, along with the Luci sequence between the CMV promoter and HRV-B3 IRES, slightly reduced RNA levels compared to inserting only the Luci sequence between the CMV promoter and HRV-B3 IRES (Fig. 4E,F). These findings indicated that the HRV-B3 IRES acts as a position-dependent negative regulatory element for the CMV promoter.

To further assess whether the Luci sequence upstream of the HRV-B3 IRES affects autocatalytic cleavage and ligation, we measured relative GFP RNA levels and circRNA junction levels to calculate circularization efficiency. Surprisingly, the Luci-containing Tornado system exhibited an increased circularization efficiency (Fig. 4G). Thus, to maximize circRNA-based protein production, we selected pCDH-Luci-Tornado-IRES-GFP (Plasmid 13) for lentiviral vector construction for subsequent experiments.

Increased circRNA-based protein expression by our modified Tornado system

To investigate the transcriptional efficacy of the pCDH-Tornado-IRES system for different protein expression, we substituted the GFP reporter with the gene encoding endothelial lipase (LIPG). The construct (pCDH-Tornado-IRES-LIPG) was transfected into HEK293T cells, and RT-qPCR analysis showed a >4500-fold increase in LIPG RNA levels compared to baseline controls (Fig. 5A), confirming the superior expression potency of the pCDH-Tornado translation platform and its potential utility for robust gene overexpression.

Various vectors have been developed for circRNA production. Among them, pLC5-ciR shuttle plasmid is specifically designed for this purpose. pCD25-ciR shares the same circularization elements as pLC5-ciR, such as modified Alu elements and binding sites for RNA-binding proteins like QKI, but its backbone is derived from pcDNA3. While these vectors have been used to produce circRNAs in previous studies, their suitability for an IRES-driven translation system remains unclear.

Moreover, to further assess the efficiency of circRNA production, the sequence of neuraminidase subtype 1 (NA1) of influenza and a C/D box (24 bp) were cloned into the modified Tornado system, pLC5-ciR, and pCD25-ciR (Fig. 5B). The C/D box RNA sequence can bind L7Ae (archaeal ribosomal protein), which is used for conjugating circRNA with exosomes (Saito et al. 2010; Kojima et al. 2018). The DNA length of the modified Tornado system construct was longer than the pLC5-ciR construct and the pCD25-ciR construct. To be noted, when the equal masses of plasmids were transfected, the molecular amounts of DNA with the modified Tornado system constructs were fewer relative to the pLC5-ciR construct and the pCD25-ciR construct (calculated based on plasmid molecular weights).

After transfection into HEK293T cells, we observed that pLC5-ciR-IRES-NA1-C/D_box produced approximately twofold higher NA1 RNA levels than pCDH-Tornado-IRES-NA1 but 0.5-fold lower than pCDH-Luci-Tornado-IRES-NA1-C/D_box (Fig. 5C). This difference may be partially attributed to the varying distances between the CMV promoter and the IRES: 324 bp for pCDH-Tornado-IRES-NA1, 500 bp for pLC5-ciR-IRES-NA1-C/D_box, and 1921 bp for pCDH-Luci-Tornado-IRES-NA1-C/D_box. Consistent with these findings, pCD25-ciR-IRES-NA1-C/D_box, based on the pcDNA3 backbone, generated minimal NA1 transcripts. Surprisingly, pLC5-ciR-IRES-NA1-C/D_box did not produce a circularization junction (Fig. 5C). Instead, it generated linear mRNA, which served

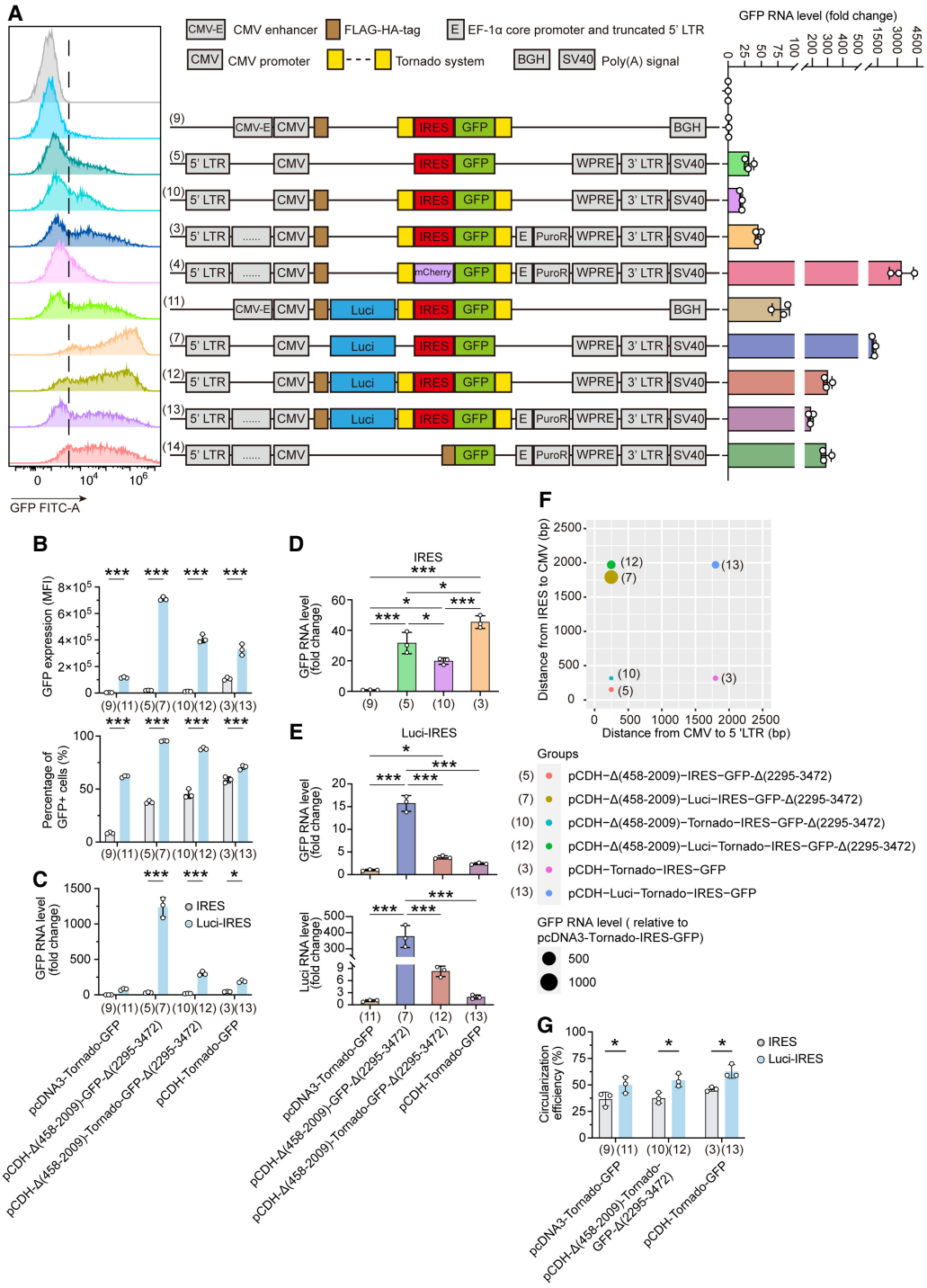

FIGURE 4. Increased distance between HRV-B3 IRES and the upstream promoter mitigates RNA-abundance downregulation. (*A*, *left*) Flow cytometry histogram plots. (*Middle*) Schematic of plasmids containing HRV-B3 IRES or mCherry. All the plasmids are numbered. The symbol (……) represents key elements, including HIV-1 Ψ, RRE, gp41 peptide, and cPPT/CTS. (*Right*) Relative GFP RNA levels in HEK293T cells transfected with the plasmids shown in the *middle* panel. (*B*) GFP expression levels (MFI) and percentage of GFP-positive cells of plasmids with or without a Luci sequence. (*C*) Relative GFP RNA levels in HEK293T cells transfected with plasmids with or without a Luci sequence. (*D*) Relative GFP RNA levels in HEK293T cells transfected with plasmids containing HRV-B3 IRES but without a Luci sequence. (*E*) Relative RNA levels of GFP and Luci in HEK293T cells transfected with plasmids containing both HRV-B3 IRES and a Luci sequence. (*F*) Scatter plot illustrating the correlation between relative GFP RNA levels and the DNA sequence length from the CMV promoter to IRES or from the CMV promoter to the 5′ LTR in the presence of HRV-B3 IRES. CMV refers to cytomegalovirus promoter. (*G*) Circularization efficiency of RNA transcribed from the Tornado translation system in plasmids with or without a Luci sequence. The data are shown as mean ± SD of at least three independent experiments, and *P*-values of <0.05 were deemed statistically significant. (*) $P < 0.05$; (***) $P < 0.001$.

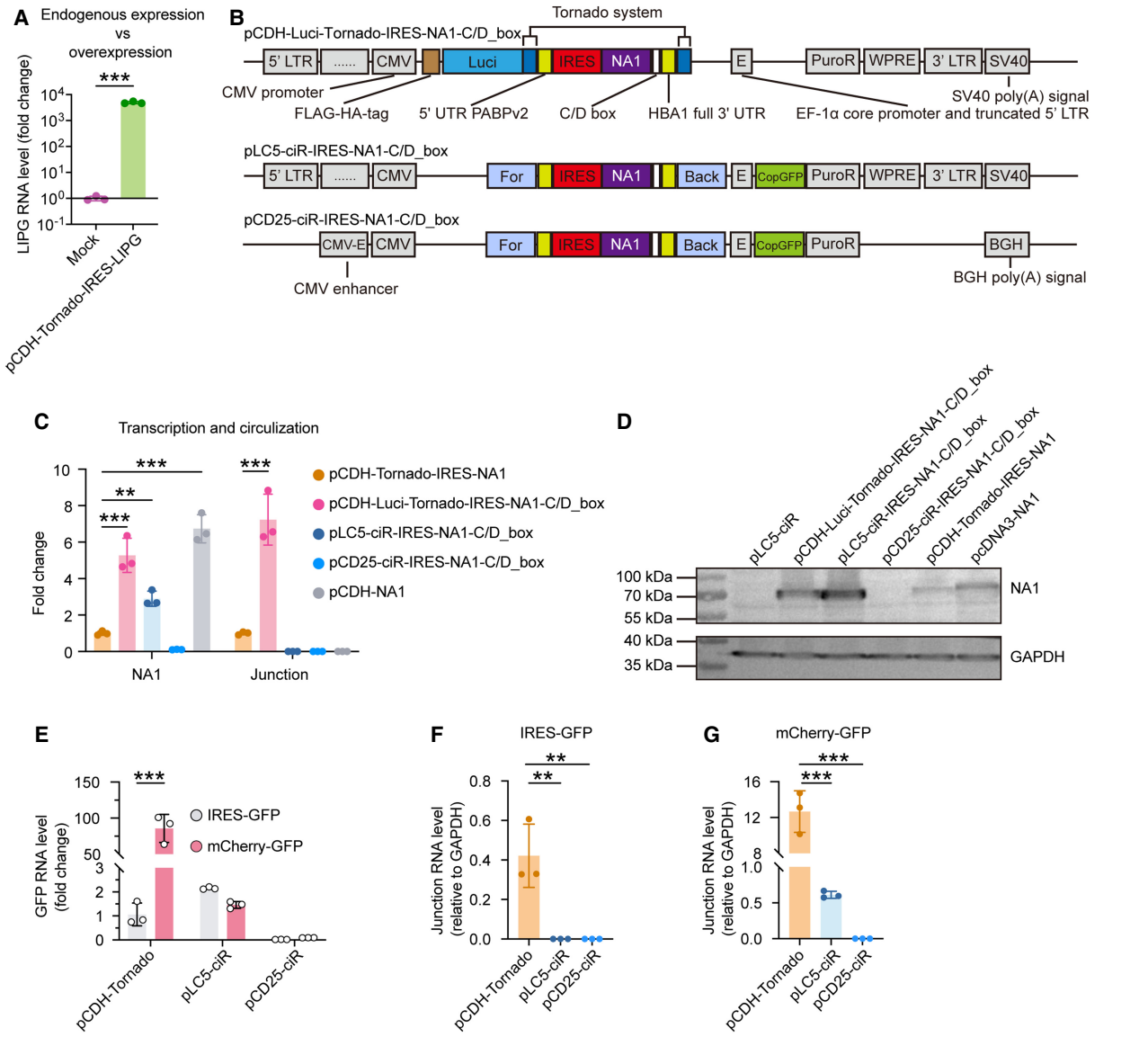

FIGURE 5. Enhanced circRNA-mediated protein expression using the modified Tornado system. (*A*) Endogenous LIPG gene overexpression using pCDH-Tornado-IRES-LIPG. Relative LIPG RNA levels were measured by RT-qPCR. (*B*) Design of the Tornado translation system in the pCDH vector, pLC5-ciR, and pCD25-ciR. The symbol (……) represents key elements, including HIV-1 Ψ, RRE, gp41 peptide, and cPPT/CTS. The Tornado system includes ribozymes and complements sequences at the 5′ and 3′ ends. (For) Forward circular frame, (Back) backward circular frame, (CopGFP) green fluorescent protein 2 from *Pontellina plumata* (ppluGFP2). (*C*) NA1 transcripts were amplified using convergent primers, while junction transcripts were amplified using divergent primers. (*D*) Western blot analysis of NA1 expression in HEK293T cells transfected with the indicated plasmids. (*E*) Relative GFP RNA levels in HEK293T cells transfected with pCDH-Tornado-IRES-GFP, pCDH-Tornado-mCherry-GFP, pLC5-ciR-IRES-GFP, pLC5-ciR-mCherry-GFP, pCD25-ciR-IRES-GFP, or pCD25-ciR-mCherry-GFP. (*F*) Relative junction RNA levels in HEK293T cells transfected with pCDH-Tornado-IRES-GFP, pLC5-ciR-IRES-GFP, or pCD25-ciR-IRES-GFP, measured using divergent primers. (*G*) Relative junction RNA levels in HEK293T cells transfected with pCDH-Tornado-mCherry-GFP, pLC5-ciR-mCherry-GFP, or pCD25-ciR-mCherry-GFP, also measured using divergent primers. The data are shown as mean ± SD of at least three independent experiments, and *P*-values of <0.05 were deemed statistically significant. (**) $P < 0.01$; (***) $P < 0.001$.

as the template for translation and resulted in the highest protein expression (Fig. 5D). Notably, pCDH-Luci-Tornado-IRES-NA1-C/D_box outperformed pLC5-ciR-IRES-NA1-C/D_box in both RNA abundance and circularization efficiency.

We further investigated whether HRV-B3 IRES reduced target RNA levels in pLC5-ciR, similar to its effect in pCDH. In these experiments, the HRV-B3 IRES was replaced with mCherry in the plasmids. After transfection, we found that HRV-B3 IRES-mediated RNA-abundance downregulation did not occur when pLC5-ciR was used as the template for exogenous circRNA production (Fig. 5E). This may be due to the presence of Alu elements in

pLC5-ciR, which are rich in secondary structures associated with transcription inhibition. Additionally, both pLC5-ciR and pCD25-ciR showed minimal ability to circularize RNA containing IRES-GFP (Fig. 5F,G). Collectively, these findings demonstrated that our modified Tornado system—comprising two functionally optimized plasmids (pCDH-Luci-Tornado-IRES-GFP [Plasmid 13] for lentiviral vector construction and pCDH-Δ(458-2009)-Luci-Tornado-IRES-GFP-Δ(2295-3472) [Plasmid 12] for enhanced protein expression)—serves as a highly effective platform for circRNA-based protein expression in mammalian cells.

DISCUSSION

The Tornado system has been extensively studied for generating circular RNAs (circRNAs) in mammalian cells, but its low circularization efficacy and abundance for large RNA inserts limits the further application to develop circRNA-based vaccines or drug delivery. Thus, it is of great importance to explore novel methods to improve the production of large RNA circularization in mammalian cells. In this study, we demonstrated that incorporating a spacer sequence of a specific length between the HRV-B3 IRES and the upstream CMV promoter significantly increases the RNA abundance and thus the expression of circRNA-based protein by the Tornado system. The modified Tornado system, which includes an appropriate distance between the IRES and the upstream CMV promoter, 5′ LTR, and WPRE, facilitates the abundance of RNAs containing Twister ribozymes flanking the RNA sequence of interest and the HRV-B3 IRES.

Several factors can influence the RNA abundance generated by the Tornado system. First, the presence of the Tornado system itself flanking a sequence of interest reduces RNA levels, as evidenced by the increased RNA abundance observed after removing the Tornado system in our study. Please note, the 5′ cap and 3′ poly(A) tail effectively protect linear mRNA in the cytoplasm from decay (Garneau et al. 2007). However, the 5′ P3 Twister U2A ribozyme in the 5′ end of the Tornado system cleaves near the 5′ end, resulting in the loss of the cap (Litke and Jaffrey 2019). Meanwhile, the 3′ P1 Twister ribozyme in the 3′ end of the Tornado system cleaves near the 3′ end, leading to the loss of the poly(A) tail (Litke and Jaffrey 2019). If the cleaved linear RNA is not circularized and is transported to the cytoplasm, it will be rapidly degraded, resulting in decreased RNA abundance. Second, the presence of the HRV-B3 IRES correlates with RNA-abundance downregulation from the Tornado system. The HCV IRES has been shown to induce RNA reduction through low RNA polymerase II occupancy in the region upstream of the IRES (Slobodin et al. 2020). Previous studies have reported that CVB3 RNA synthesis is inhibited by AU-rich element degradation factor 1 (AUF1 or hnRNP D), although AUF1 does not promote CVB3 RNA decay (Ullmer and Semler 2018). Additionally, AUF1 negatively regulates CVB3 IRES-driven translation, potentially acting as a negative IRES *trans*-acting factor by competing for IRES binding in its RNA form. However, no studies have reported that the quantity of IVT RNA depends on the presence of an IRES, suggesting that T7 RNA polymerase is not affected by IRES. Thus, the RNA-abundance downregulation exerted by the HRV-B3 IRES in its DNA form may be promoter-specific or dependent on binding to specific proteins in a certain underlying mechanism. In this study, we found that the downregulation effect of RNA abundance by the HRV-B3 IRES is position-dependent. For example, compared to that of pCDH-Tornado-IRES-GFP (Plasmid 3), the distance from the HRV-B3 IRES to the 5′ LTR of pCDH-Δ(458-2009)-Tornado-IRES-GFP-Δ(2295-3472) (Plasmid 10) is shorter, while the distance from the HRV-B3 IRES to the CMV promoter remained same, but the relative GFP RNA level transcribed from pCDH-Δ(458-2009)-Tornado-IRES-GFP-Δ(2295-3472) (Plasmid 10) was lower than that from pCDH-Tornado-IRES-GFP (Plasmid 3). This reduction in RNA abundance may be attributed to the decreased spatial distance between the IRES and the 5′ LTR, which hinders transcription initiation (Miyoshi et al. 1998). This finding underscores the crucial role of transcription initiation at the 5′ LTR in increasing RNA levels. More importantly, we observed a significant increase in RNA levels produced by the Tornado system when the distance between the HRV-B3 IRES and the upstream CMV promoter was extended in an appropriate length. Interestingly, given the inherent Tornado system-mediated faster mRNA degradation (Litke and Jaffrey 2019) and IRES-mediated accelerated mRNA instability (Slobodin et al. 2020), this rapid processing ensures immediate removal of inserted sequences from mature transcripts, effectively decoupling these elements from potential post-transcriptional regulation. Thus, the resultant transcripts are structurally indistinguishable from native mRNAs in terms of stability determinants, and consequently, the increased RNA level by our modified Tornado system should be mainly due to a transcriptional enhancement. Together, these findings suggest that the IRES not only functions as a translation driver in its RNA form but also acts as a position-dependent negative regulatory element in its DNA form.

In this study, we also studied the circRNA production using pLC5-ciR, a commercialized and optimized backsplicing system plasmid (Huang et al. 2024). This system is designed to generate circRNA by leveraging endogenous gene expression mechanisms, including Alu elements and QKI. However, our experiments revealed that the predominant product from pLC5-ciR was linear RNA but not circRNA, likely due to the more efficient forward splicing reaction. This observation aligns with previous report that backsplicing systems predominantly generate linear forward splicing products (Unti and Jaffrey 2024). In contrast, the Tornado system can produce circRNAs with a circularization efficiency

exceeding 36%, and we further increased it to over 50% by adjusting the distance between the HRV-B3 IRES and the upstream CMV promoter. Therefore, our modified Tornado system with the superior circularization efficiency is highly recommended for scenarios requiring the generation of large and diverse circRNAs in cells. For example, circRNA-loaded exosomes can be harvested after donor cells are transfected with this modified Tornado system.

Although our modified Tornado translation system significantly increased circRNA-based expression level compared to its parental version, the spacer sequence—a nonessential luciferase ORF separating the IRES from the upstream promoter—might introduce interpretative ambiguity. (1) It remains unclear whether the enhancement effect by the inserted spacer is sequence-specific, particularly regarding how replacement of the luciferase ORF sequence with alternative *cis*-acting elements would affect this phenomenon. (2) Given an additional 2289 bp insertion in the parental expression vector and an additional 1623 bp insertion in the parental shuttle vector, the recombinant lentiviruses containing this modified Tornado system might potentially have a compromised capacity for its packaging efficiency and carrying therapeutic transgenes. (3) The transfection efficacy can be decreased by the enlarged constructs due to an inverse relationship between the length of constructs and cellular internalization rates. Thus, future research should prioritize the intervals between the CMV promoter and IRES element with a noncoding sequence and finely adjust the length of the constructs for optimized therapeutic implementations. In addition, although supported by both our data and another report (Slobodin et al. 2020) for the different IRES elements of HCV, HRV-B3, and CVB3, the generalizability of the conclusion that IRES element can play a role in RNA-abundance downregulation should be examined with a broader interpretation, since there are more than 17,200 documented IRES polymorphism and variations in flanking regulatory regions (Chen et al. 2021). Importantly, the exact mechanism by which the IRES element downregulates RNA abundance remains an unresolved important area and warrants further investigation.

Overall, we developed a modified Tornado system for improving circRNA-based protein expression, and further elucidated the dual roles of HRV-B3 IRES in negative RNA-abundance regulation and positive RNA circularization in mammalian cells. This modified system offers a promising platform for the development of circRNA-based therapeutics and vaccines.

MATERIALS AND METHODS

Cell lines

HEK293T cell line was maintained in our laboratory. HEK293T cells were cultured in Dulbecco's modified Eagle medium (DMEM), with 10% fetal bovine serum (ExCell), supplemented with 1% penicillin–streptomycin in 5% CO_2 incubator at 37°C.

Plasmid construction

For in vitro circRNA transcription, plasmids were constructed by synthesizing and cloning the following components into pUC57: the T7 RNA polymerase promoter, 5′ and 3′ homology arms, group I intron sequences, exon sequences, spacer sequences, IRES, GFP, and other regulatory elements. The circRNA containing CVB3 IRES sequence was designed based on Qu's work (Qu et al. 2022), while the HRV-B3 IRES sequence, including an eIF4G-binding aptamer, 5′ UTR PABPv2 spacer, and HBA1 full 3′ UTR, was adapted from Chen's work (Chen et al. 2023).

For the Tornado translation system, the Tornado sequence was synthesized and cloned into the pcDNA3 backbone, generating the pcDNA3-Tornado plasmid. CVB3 and HRV-B3 IRES sequences, along with their spacer elements, were PCR-amplified and cloned into pcDNA3-Tornado to create pcDNA3-Tornado-CVB3_IRES and pcDNA3-Tornado-HRV-B3_IRES. GFP, Luci, the neuraminidase from the H1N1 influenza virus (NA1), and mCherry coding sequences were subsequently cloned into these plasmids. Additional constructs were generated using seamless cloning with the ClonExpress Ultra One Step Cloning Kit V2 (Vazyme C116) and cloned into the pCDH-CMV-MCS-EF1-Puro plasmid (hereafter referred to as pCDH), pLC5-ciR (Geneseed Biotech, Guangzhou, China), or pCD25-ciR (Geneseed Biotech). These sequences are shown in Supplemental Table S1.

Production and purification of circRNA

The production and purification of circRNAs was performed according to previous reports (Wesselhoeft et al. 2018; Qu et al. 2022). Briefly, linearized plasmid templates were used for IVT with the HiScribe T7 High Yield RNA Synthesis Kit (NEB E2040S). Post-IVT, RNA products were treated with DNase I (NEB M0303S) for 30 min to remove DNA templates. Circularization was catalyzed by adding GTP (2 mM final concentration) and incubating at 55°C for 15 min. RNA was purified using the Monarch RNA Cleanup Kit (NEB T2040L), heated at 70°C for 3 min, and cooled on ice. Recircularization was performed with GTP and T4 DNA Ligase Reaction Buffer, followed by final column purification.

Transfection

HEK293T cells (3×10^5 cells/well) were seeded in 12-well plates and transfected with 1 µg of circRNA or plasmid, using Lipofectamine MessengerMAX (Invitrogen LMRNA003) for circRNA or jetPRIME (Polyplus-transfection 101000046) for DNA plasmids. At 48 h post-transfection, fluorescence signals were imaged using an inverted fluorescence microscope (Axio Observer 3, Carl Zeiss), and cells were collected for further analysis.

RNA quantification

RNA levels in transfected HEK293T cells were quantified by RT-qPCR. Total RNA was extracted using the Universal RNA

Purification Kit (EZBioscience EZB-RN4), reverse transcribed, and amplified using Hieff qPCR SYBR Green Master Mix (Yeasen 11202ES08). GAPDH served as the internal reference. Primer sequences are listed in Supplemental Table S2. Measurements of RNA levels for GFP, Luciferase, and NA1 represented total RNA abundance, including both linear and circular RNA forms.

Circularization efficiency of RNA was quantified using a previously published qPCR-based method (Amer and Almajhdi 2011). To amplify the cDNA of the target circRNA, which included the GFP sequence, the circRNA junction region, and the IRES/mCherry sequence, we used forward primers specific to the 5′ GFP region and reverse primers specific to the 3′ IRES/mCherry region. The amplified cDNA sequences were subsequently cloned into the pcDNA3 vector. These plasmids, harboring the target sequences, served as DNA standards for qPCR quantification. The plasmids were 10-fold serially diluted starting with a 1:20 dilution (the primary concentrations were about 1×10^{10} copies/μL). These diluted plasmids were used as templates for qPCR. The cycle threshold (C_t) values obtained from the qPCR reactions were used to construct standard curves. Specifically, the C_t values were plotted against the logarithm of the plasmid copy numbers to generate the standard curves. Total RNA was extracted from HEK293T cells transfected with plasmids harboring either IRES-positive or IRES-negative plasmids, as well as plasmids with or without the inserted sequences. The cDNA was synthesized from the total RNA. The C_t values for the cDNA samples were determined via qPCR. Using the standard curves generated from the plasmid standards, the absolute copy numbers of the target RNA (GFP and circRNA junction) in the samples were calculated. The circularization efficiency was calculated as the ratio of the copy number of the circRNA junction to the copy number of GFP.

Flow cytometry analysis

Transfected cells were washed twice with PBS, resuspended in 300 μL PBS, and filtered through a 200-mesh filter. Samples were analyzed on a CytoFlex S (Beckman Coulter).

Luciferase assay

As previously reported (Zhao et al. 2022; Li et al. 2023), HEK293T cells transfected with pcDNA3-Luci or pcDNA3-Tornado-IRES-Luci were detected for bioluminescence using a GloMax 96 luminometer (Promega) with a bright-light luciferase assay system.

Western blot

For detecting NA1 protein expression, the HEK293T cells were cultured in 6-well plates, and transfected with pcDNA3-NA1, pCDH-Tornado-IRES-NA1, pCDH-Luci-Tornado-IRES-NA1-C/D_box, pLC5-ciR, pLC5-ciR-IRES-NA1-C/D_box, or pCD25-ciR-IRES-C/D_box for 48 h. These cells were then lysed, and proteins were separated by SDS-PAGE for western blot analysis as previously reported (Han et al. 2024). All loading controls were proteins from the same gel and membrane as the proteins under examination.

Statistical analysis

Two-tailed Student's *t*-tests were used for two-group comparisons. Multigroup comparisons were performed using one- or two-way ANOVA followed. Data are presented as mean ± SD, with $P < 0.05$ considered statistically significant.

SUPPLEMENTAL MATERIAL

Supplemental material is available for this article.

ACKNOWLEDGMENTS

This work was supported by the National Natural Science Foundation of China (82472267, 82271786), Science and Technology Planning Project of Guangdong Province, China (2021B1212040017, 2022B1212060001, 2023B1212130001, 2024B1212160001), Shenzhen Science and Technology Program (ZDSYS20230626091203007), Sanming Project of Medicine in Shenzhen Nanshan (no. SZSM202103008), and Key Subject of Nanshan District of Shenzhen for AIDS surveillance and prevention. We thank Ziyu Wen of the University of Pennsylvania and Minjuan Shi of the Caijun Sun laboratory for insightful comments and suggestions.

Received February 26, 2025; accepted August 28, 2025.

REFERENCES

Amer HM, Almajhdi FN. 2011. Development of a SYBR Green I based real-time RT-PCR assay for detection and quantification of bovine coronavirus. *Mol Cell Probes* **25:** 101–107. doi:10.1016/j.mcp.2011.03.001

Chen CY, Sarnow P. 1995. Initiation of protein synthesis by the eukaryotic translational apparatus on circular RNAs. *Science* **268:** 415–417. doi:10.1126/science.7536344

Chen YG, Kim MV, Chen X, Batista PJ, Aoyama S, Wilusz JE, Iwasaki A, Chang HY. 2017. Sensing self and foreign circular RNAs by intron identity. *Mol Cell* **67:** 228–38.e5. doi:10.1016/j.molcel.2017.05.022

Chen YG, Chen R, Ahmad S, Verma R, Kasturi SP, Amaya L, Broughton JP, Kim J, Cadena C, Pulendran B, et al. 2019. *N*6-methyladenosine modification controls circular RNA immunity. *Mol Cell* **76:** 96–109.e9. doi:10.1016/j.molcel.2019.07.016

Chen CK, Cheng R, Demeter J, Chen J, Weingarten-Gabbay S, Jiang L, Snyder MP, Weissman JS, Segal E, Jackson PK, et al. 2021. Structured elements drive extensive circular RNA translation. *Mol Cell* **81:** 4300–18.e13. doi:10.1016/j.molcel.2021.07.042

Chen R, Wang SK, Belk JA, Amaya L, Li Z, Cardenas A, Abe BT, Chen CK, Wender PA, Chang HY. 2023. Engineering circular RNA for enhanced protein production. *Nat Biotechnol* **41:** 262–272. doi:10.1038/s41587-022-01393-0

Chen L, Song L, Yang J, Li T, Ju R, Sun C, Xie Z. 2025. Development and comprehensive evaluation of scarless circularization systems for circular RNA therapeutics. *Mol Ther Nucleic Acids* **36:** 102587. doi:10.1016/j.omtn.2025.102587

Conn SJ, Pillman KA, Toubia J, Conn VM, Salmanidis M, Phillips CA, Roslan S, Schreiber AW, Gregory PA, Goodall GJ. 2015. The RNA binding protein quaking regulates formation of circRNAs. *Cell* **160:** 1125–1134. doi:10.1016/j.cell.2015.02.014

Dubin RA, Kazmi MA, Ostrer H. 1995. Inverted repeats are necessary for circularization of the mouse testis *Sry* transcript. *Gene* **167:** 245–248. doi:10.1016/0378-1119(95)00639-7

Filipowicz W, Shatkin AJ. 1983. Origin of splice junction phosphate in tRNAs processed by HeLa cell extract. *Cell* **32:** 547–557. doi:10.1016/0092-8674(83)90474-9

Garneau NL, Wilusz J, Wilusz CJ. 2007. The highways and byways of mRNA decay. *Nat Rev Mol Cell Biol* **8:** 113–126. doi:10.1038/nrm2104

Han Z, Mai Q, Zhao Y, Liu X, Cui M, Li M, Chen Y, Shu Y, Gan J, Pan W, et al. 2024. Mosaic neuraminidase-based vaccine induces antigen-specific T cell responses against homologous and heterologous influenza viruses. *Antiviral Res* **230:** 105978. doi:10.1016/j.antiviral.2024.105978

Huang Q, Chu Z, Wang Z, Li Q, Meng S, Lu Y, Ma K, Cui S, Hu W, Zhang W, et al. 2024. circCDK13-loaded small extracellular vesicles accelerate healing in preclinical diabetic wound models. *Nat Commun* **15:** 3904. doi:10.1038/s41467-024-48284-3

Ibrahim H, Wilusz J, Wilusz CJ. 2008. RNA recognition by 3′-to-5′ exonucleases: the substrate perspective. *Biochim Biophys Acta* **1779:** 256–265. doi:10.1016/j.bbagrm.2007.11.004

Ivanov A, Memczak S, Wyler E, Torti F, Porath HT, Orejuela MR, Piechotta M, Levanon EY, Landthaler M, Dieterich C, et al. 2015. Analysis of intron sequences reveals hallmarks of circular RNA biogenesis in animals. *Cell Rep* **10:** 170–177. doi:10.1016/j.celrep.2014.12.019

Jeck WR, Sorrentino JA, Wang K, Slevin MK, Burd CE, Liu J, Marzluff WF, Sharpless NE. 2013. Circular RNAs are abundant, conserved, and associated with ALU repeats. *RNA* **19:** 141–157. doi:10.1261/rna.035667.112

Knudsen S. 1999. Promoter2.0: for the recognition of PolII promoter sequences. *Bioinformatics* **15:** 356–361. doi:10.1093/bioinformatics/15.5.356

Kojima R, Bojar D, Rizzi G, Hamri GC, El-Baba MD, Saxena P, Ausländer S, Tan KR, Fussenegger M. 2018. Designer exosomes produced by implanted cells intracerebrally deliver therapeutic cargo for Parkinson's disease treatment. *Nat Commun* **9:** 1305. doi:10.1038/s41467-018-03733-8

Kramer MC, Liang D, Tatomer DC, Gold B, March ZM, Cherry S, Wilusz JE. 2015. Combinatorial control of *Drosophila* circular RNA expression by intronic repeats, hnRNPs, and SR proteins. *Genes Dev* **29:** 2168–2182. doi:10.1101/gad.270421.115

Laski FA, Fire AZ, RajBhandary UL, Sharp PA. 1983. Characterization of tRNA precursor splicing in mammalian extracts. *J Biol Chem* **258:** 11974–11980. doi:10.1016/S0021-9258(17)44327-4

Li Z, Huang C, Bao C, Chen L, Lin M, Wang X, Zhong G, Yu B, Hu W, Dai L, et al. 2015. Exon-intron circular RNAs regulate transcription in the nucleus. *Nat Struct Mol Biol* **22:** 256–264. doi:10.1038/nsmb.2959

Li M, Yang L, Wang C, Cui M, Wen Z, Liao Z, Han Z, Zhao Y, Lang B, Chen H, et al. 2023. Rapid induction of long-lasting systemic and mucosal immunity via thermostable microneedle-mediated chitosan oligosaccharide-encapsulated DNA nanoparticles. *ACS Nano* **17:** 24200–24217. doi:10.1021/acsnano.3c09521

Liang D, Wilusz JE. 2014. Short intronic repeat sequences facilitate circular RNA production. *Genes Dev* **28:** 2233–2247. doi:10.1101/gad.251926.114

Litke JL, Jaffrey SR. 2019. Highly efficient expression of circular RNA aptamers in cells using autocatalytic transcripts. *Nat Biotechnol* **37:** 667–675. doi:10.1038/s41587-019-0090-6

Lu Z, Filonov GS, Noto JJ, Schmidt CA, Hatkevich TL, Wen Y, Jaffrey SR, Matera AG. 2015. Metazoan tRNA introns generate stable circular RNAs in vivo. *RNA* **21:** 1554–1565. doi:10.1261/rna.052944.115

Miyoshi H, Blömer U, Takahashi M, Gage FH, Verma IM. 1998. Development of a self-inactivating lentivirus vector. *J Virol* **72:** 8150–8157. doi:10.1128/jvi.72.10.8150-8157.1998

Obi P, Chen YG. 2021. The design and synthesis of circular RNAs. *Methods* **196:** 85–103. doi:10.1016/j.ymeth.2021.02.020

Puttaraju M, Been MD. 1992. Group I permuted intron-exon (PIE) sequences self-splice to produce circular exons. *Nucleic Acids Res* **20:** 5357–5364. doi:10.1093/nar/20.20.5357

Qu L, Yi Z, Shen Y, Lin L, Chen F, Xu Y, Wu Z, Tang H, Zhang X, Tian F, et al. 2022. Circular RNA vaccines against SARS-CoV-2 and emerging variants. *Cell* **185:** 1728–44.e16. doi:10.1016/j.cell.2022.03.044

Saito H, Kobayashi T, Hara T, Fujita Y, Hayashi K, Furushima R, Inoue T. 2010. Synthetic translational regulation by an L7Ae-kink-turn RNP switch. *Nat Chem Biol* **6:** 71–78. doi:10.1038/nchembio.273

Slobodin B, Bahat A, Sehrawat U, Becker-Herman S, Zuckerman B, Weiss AN, Han R, Elkon R, Agami R, Ulitsky I, et al. 2020. Transcription dynamics regulate poly(A) tails and expression of the RNA degradation machinery to balance mRNA levels. *Mol Cell* **78:** 434–44.e5. doi:10.1016/j.molcel.2020.03.022

Tanaka N, Chakravarty AK, Maughan B, Shuman S. 2011. Novel mechanism of RNA repair by RtcB via sequential 2′,3′-cyclic phosphodiesterase and 3′-phosphate/5′-hydroxyl ligation reactions. *J Biol Chem* **286:** 43134–43143. doi:10.1074/jbc.M111.302133

Ullmer W, Semler BL. 2018. Direct and indirect effects on viral translation and RNA replication are required for AUF1 restriction of enterovirus infections in human cells. *mBio* **9:** e01669-18. doi:10.1128/mBio.01669-18

Unti MJ, Jaffrey SR. 2024. Highly efficient cellular expression of circular mRNA enables prolonged protein expression. *Cell Chem Biol* **31:** 163–176. doi:10.1016/j.chembiol.2023.09.015

Wesselhoeft RA, Kowalski PS, Anderson DG. 2018. Engineering circular RNA for potent and stable translation in eukaryotic cells. *Nat Commun* **9:** 2629. doi:10.1038/s41467-018-05096-6

Wesselhoeft RA, Kowalski PS, Parker-Hale FC, Huang Y, Bisaria N, Anderson DG. 2019. RNA circularization diminishes immunogenicity and can extend translation duration *in vivo*. *Mol Cell* **74:** 508–20.e4. doi:10.1016/j.molcel.2019.02.015

Yue X, Zhong C, Cao R, Liu S, Qin Z, Liu L, Zhai Y, Luo W, Lian Y, Zhang M, et al. 2024. CircRNA based multivalent neuraminidase vaccine induces broad protection against influenza viruses in mice. *NPJ Vaccines* **9:** 170. doi:10.1038/s41541-024-00963-4

Zhang XO, Wang HB, Zhang Y, Lu X, Chen LL, Yang L. 2014. Complementary sequence-mediated exon circularization. *Cell* **159:** 134–147. doi:10.1016/j.cell.2014.09.001

Zhao J, Chen J, Wang C, Liu Y, Li M, Li Y, Li R, Han Z, Wang J, Chen L, et al. 2022. Kynurenine-3-monooxygenase (KMO) broadly inhibits viral infections via triggering NMDAR/Ca^{2+} influx and CaMKII/IRF3-mediated IFN-β production. *PLoS Pathog* **18:** e1010366. doi:10.1371/journal.ppat.1010366

See the following page for ***Meet the First Author***

MEET THE FIRST AUTHOR

Mingting Cui

***Meet the First Author(s)* is an editorial feature within *RNA*, in which the first author(s) of research-based papers in each issue have the opportunity to introduce themselves and their work to readers of *RNA* and the RNA research community. Mingting Cui is the first author of this paper, "Development of a modified RNA circularization system to improve circRNA-based protein expression in mammalian cells." Mingting recently earned her Master's degree after completing her academic research in Professor Caijun Sun's laboratory at Sun Yat-sen University, China. Her work focused on optimizing a large circular RNA expression system—specifically the Tornado translation system—by developing molecular design strategies to enhance circular RNA abundance and subsequent protein expression.**

What are the major results described in your paper, and how do they impact this branch of the field?

This paper reports a novel finding that the HRV-B3 internal ribosomal entry site (IRES) functions as a position-dependent negative regulator of the upstream promoter, but this inhibitory effect can be mitigated by inserting a spacer sequence between the IRES and the promoter. This strategy offers a highly effective alternative for enhancing the expression of large circular RNAs in mammalian cells.

What led you to study RNA or this aspect of RNA science?

To develop novel mRNA-based therapeutic and vaccine strategies, I previously established a stable cell line capable of expressing large, protein-coding circular RNAs using a pCDH shuttle plasmid system. During this process, I observed that the Tornado translation system generated a markedly enhanced GFP signal after being cloned into the pCDH vector, highlighting its potential for high-level circular RNA expression.

During the course of these experiments, were there any surprising results or particular difficulties that altered your thinking and subsequent focus?

Although a strong GFP signal was observed in cells transfected with the Tornado translation system cloned into the pCDH plasmid, no signal was observed in cells following transduction with the corresponding lentiviral construct. I realized there must be something different between these constructs.

What are some of the landmark moments that provoked your interest in science or your development as a scientist?

I was particularly excited to discover that the low-yield limitation associated with encoding large sequences in the Tornado system could be overcome by mitigating the inhibitory effect of the HRV-B3 IRES on RNA abundance—a finding that greatly satisfied my scientific curiosity.

If you were able to give one piece of advice to your younger self, what would that be?

Maintain your curiosity.

Are there specific individuals or groups who have influenced your philosophy or approach to science?

My undergraduate advisor Dr. Caijun Sun has played a huge role in shaping me as a scientist.

What are your subsequent near- or long-term career plans?

I plan on working as a healthcare professional at an exciting new startup, with a mission to advance human health.

Development of a modified RNA circularization system to improve circRNA-based protein expression in mammalian cells

Mingting Cui, Shunran Li, Yuhang Han, et al.

RNA 2025 31: 1912-1926 originally published online September 11, 2025
Access the most recent version at doi:10.1261/rna.080733.125